High-frequency oscillations in human and monkey neocortex during the wake–sleep cycle

Michel Le Van Quyen[a,1], Lyle E. Muller II[b,1], Bartosz Telenczuk[c,1], Eric Halgren[d,e], Sydney Cash[f,g], Nicholas G. Hatsopoulos[h], Nima Dehghani[i,j,2], and Alain Destexhe[c,2]

[a]Institut du Cerveau et de la Moelle Epinière, UMRS 1127, CNRS UMR 7225, Hôpital de la Pitié-Salpêtrière, 75013 Paris, France; [b]Computational Neurobiology Laboratory, Salk Institute, La Jolla, CA 92037; [c]Laboratory of Computational Neuroscience, Unité de Neurosciences, Information, et Complexité, CNRS, 91190 Gif-sur-Yvette, France; [d]Multimodal Imaging Laboratory, Department of Neurosciences, University of California, San Diego, La Jolla, CA 92093; [e]Multimodal Imaging Laboratory, Department of Radiology, University of California, San Diego, La Jolla, CA 92093; [f]Department of Neurology, Massachusetts General Hospital, Boston, MA 02114; [g]Department of Neurology, Harvard Medical School, Boston, MA 02115; [h]Department of Organismal Biology and Anatomy, Committee on Computational Neuroscience, University of Chicago, Chicago, IL 60637; [i]Wyss Institute for Biologically Inspired Engineering, Harvard University, Boston, MA 02115; and [j]New England Complex Systems Institute, Cambridge, MA 02142

Edited by Charles F. Stevens, The Salk Institute for Biological Studies, La Jolla, CA, and approved June 21, 2016 (received for review December 2, 2015)

Beta (β)- and gamma (γ)-oscillations are present in different cortical areas and are thought to be inhibition-driven, but it is not known if these properties also apply to γ-oscillations in humans. Here, we analyze such oscillations in high-density microelectrode array recordings in human and monkey during the wake–sleep cycle. In these recordings, units were classified as excitatory and inhibitory cells. We find that γ-oscillations in human and β-oscillations in monkey are characterized by a strong implication of inhibitory neurons, both in terms of their firing rate and their phasic firing with the oscillation cycle. The β- and γ-waves systematically propagate across the array, with similar velocities, during both wake and sleep. However, only in slow-wave sleep (SWS) β- and γ-oscillations are associated with highly coherent and functional interactions across several millimeters of the neocortex. This interaction is specifically pronounced between inhibitory cells. These results suggest that inhibitory cells are dominantly involved in the genesis of β- and γ-oscillations, as well as in the organization of their large-scale coherence in the awake and sleeping brain. The highest oscillation coherence found during SWS suggests that fast oscillations implement a highly coherent reactivation of wake patterns that may support memory consolidation during SWS.

excitation | inhibition | state-dependent firing | wave propagation | synchrony

Neocortical beta (β)- and gamma (γ)-oscillations have been largely studied in the context of action/cognition during wakefulness (1–3). Although numerous studies have focused intensely on the information-processing role of β and γ during wakefulness, these rhythms do also occur during deep anesthesia and natural sleep (4–6). Additionally, although very-high-frequency allocortical oscillations (e.g., ripples at 80–200 Hz and fast ripples at 200–500 Hz in rodent/human hippocampus) have been thoroughly implicated in sleep-dependent memory consolidation (ref. 7 and reviewed in refs. 8 and 9), the occurrence and role of neocortical β- and γ-oscillations during sleep remain largely unexplored and related studies have been limited to macroscopic (whole-brain) scales (e.g., ref. 10). A recent study using microwires and intracranial electroencephalography (iEEG) recordings in the neocortex of epileptics has verified the strong presence of γ-oscillations during slow-wave sleep (SWS) (11). That study also showed a marked increase of spiking during γ, a suggestive indicator of association with cortical UP states. Here, we evaluate the presence of neocortical β- and γ-oscillations during the wake–sleep cycle at the level of local circuitry using dense 2D multielectrode recordings with identified excitatory and inhibitory cells (12, 13).

Experimental and theoretical studies suggest that thalamocortical oscillations (including β and γ) are generated through a combination of intrinsic mechanisms involving the interplay between different ionic currents and extrinsic interaction of inhibitory and excitatory cell populations (14). Mechanistically, it has been shown that the temporal interplay of synaptic excitation and inhibition (15) and the dynamic balance of ensemble excitation and inhibition (13) shape the neocortical network activity during different states [wakefulness, SWS, and rapid eye movement (REM)]. Specifically, studies of hippocampal and entorhinal cortex point to a link between phasic discharge of fast-spiking (FS) interneurons and the γ-cycle (16–19), and show how the excitation/inhibition balance modulates γ-oscillations (20). Both experimental and simulation studies frame β-oscillations as inhibition-based rhythms as well (21, 22). Here, we show how the interplay of neocortical inhibitory (FS) and excitatory [regular-spiking (RS)] activity is related to these oscillations during the sleep–wake cycle. Additionally, we examine the spiking relation with local field potentials (LFPs) to better elucidate the spatiotemporal organization of inhibitory/excitatory spiking during neocortical β- and γ-wave propagation and coherence in the sleep–wake cycle.

Results

In what follows, we first examine how excitatory and inhibitory units correlate with γ- and β-oscillations. Next, we analyze their spatial coherence and spatiotemporal organization, comparing wake and sleep states.

Prominent Presence of High-Frequency Oscillations During the Wake–Sleep Cycle. In both man and monkey, we detected numerous γ- and β-oscillatory events in multielectrode recordings during both wakefulness and sleep states (Fig. 1 and Fig. S1). In both raw and

Significance

We show in humans that in comparison to excitatory cells, inhibitory neurons have a stronger spiking activity during γ oscillations in the wake–sleep cycle. During β-oscillations in monkey neocortex, inhibitory cells show more active firing. Unlike excitatory cells, inhibitory cells show correlations during slow-wave sleep fast oscillations over several millimeters in the neocortex. During both wake and sleep, β- and γ-waves systematically propagate with a dominant trajectory across the array with similar velocities. These findings suggest that inhibition-driven β- and γ-oscillations may contribute to the reactivation of information during sleep through orchestrating highly coherent spiking activity patterns.

Author contributions: M.L.V.Q., N.D., and A.D. designed research; E.H., S.C., and N.G.H. performed experiments; M.L.V.Q., L.E.M., B.T., and N.D. analyzed data; and N.D. and A.D. wrote the paper.

The authors declare no conflict of interest.

This article is a PNAS Direct Submission.

[1]M.L.V.Q., L.E.M., and B.T. contributed equally to this work.

[2]To whom correspondence may be addressed. Email: nima.dehghani@wyss.harvard.edu or destexhe@unic.cnrs-gif.fr.

This article contains supporting information online at www.pnas.org/lookup/suppl/doi:10.1073/pnas.1523583113/-/DCSupplemental.

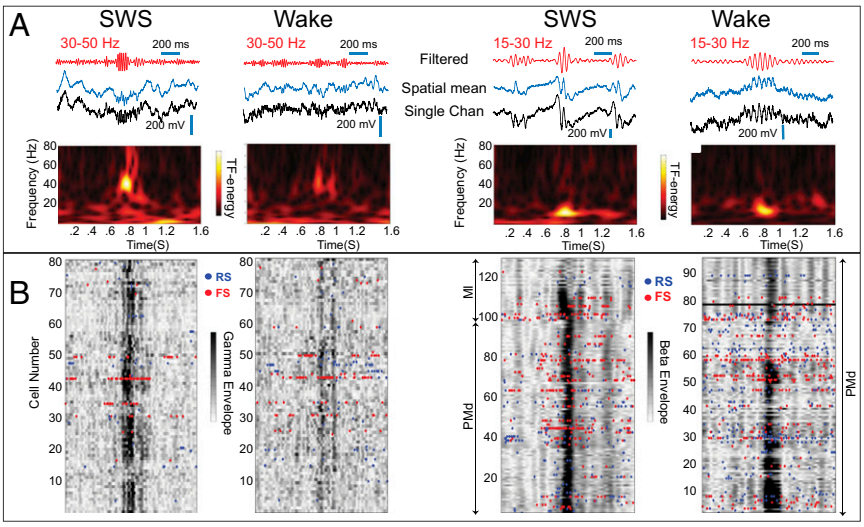

Fig. 1. γ- and β-Oscillations during sleep and wakefulness. (*A*) γ- and β-oscillations were identified in LFPs during SWS and wakefulness (Wake) in both human and monkey. The raw and filtered traces (*Top*) and wavelet time frequency of the sample epoch (*Bottom*) are shown. Chan, channel. (*B*) These oscillations most frequently appeared at about the same time across the array, forming broad spatial patterns. Red and blue dots are spiking from inhibitory FS and excitatory RS cells recorded with the same electrodes from which the LFP oscillatory envelope is calculated.

filtered signal (β- and γ-range), large-amplitude fast and transient oscillations appeared in many channels as discrete events that were clearly distinguishable from background activity (Table S1). In the temporal neocortex of humans, γ (30–50 Hz) was the main high-frequency oscillatory event, with similar dominant frequencies and interepisode intervals across all stages of vigilance (Table S1). In monkey premotor dorsal (PMd) and motor (MI) neocortical recordings, β (15–30 Hz) was the prominent high-frequency oscillation, with similar properties across the sleep–wake cycle (Table S2). Individual examples of β- and γ-events are illustrated in Figs. S2 and S3.

Firing Probability of FS and RS Cells in Relation to β and γ. After categorizing the cells into the two FS inhibitory and RS excitatory groups, we tested their firing relation to the β- and γ-oscillations in wake and sleep states. During both β- and γ-events, a larger proportion of FS cells showed high firing probability (72% for γ and 65% for β). This higher firing rate during oscillation was not restricted to FS cells; some RS cells showed higher firing probability as well (36% for γ and 32% for β; heat maps in Fig. 2). Similar firing behaviors were seen across the different stages of vigilance. Firing properties of FS and RS cells during different states are summarized in Table S3.

Heterogeneity of Spiking Pattern During β and γ. Evaluation of the firing probability of a given cell across different (β and γ) oscillatory events shows that these cells have remarkable heterogeneity of response patterns (Fig. 2, *Right*). Some cells (either FS or RS; such as 33 and 56 in γ-events shown in Fig. 2, *Left*) show a highly modulated firing rate (with respect to the oscillatory event timing), and some do not show the same stereotypical behavior across different events. Cells that do not show any strong firing changes during the oscillations manifest distinctively different firing patterns. For example, some of these cells show higher firing rates in comparison to the others (such as sparse firing of cells 55 and 57 versus the stochastic yet higher firing rate of cells 16, 2, and 154 shown in Fig. 2). In summary, both FS and RS cells show heterogeneous patterns of firing, with a larger proportion of FS cells showing a higher firing rate during β or γ, either in a tight stereotypical fashion or more variably.

Phase-Locking of FS and RS Cells Relative to β and γ. As shown above (Fig. 2), firing of FS and RS cells shows changes during the oscillatory β- and γ-events. An extracted phase of the LFP (from the electrode that recorded spiking of a given cell) shows that both FS and RS cells have variable degrees of phase-locking (evaluated with the Rayleigh test at $P < 0.05$; Fig. 3). The percentage of cells for which firing was phase-locked to β- and γ-oscillations varied in different behavioral states; it was highest during SWS (22% of FS and 6% of RS cells for γ, 42% of FS and 28% of RS cells for β) and lowest during wake (13% of FS and 9% of RS cells for γ, 4% of FS and 2% of RS cells for β). In all states, in both β and γ, a larger proportion of FS cells exhibited significant phase-locking than RS cells. The degree of this phase-locking was variable from cell to cell, with some showing strong stereotypical modulation (e.g., cell 57 in β-oscillation in Fig. 3*A*, *Right*). Note that a given cell does not necessarily show strict tuning to a given frequency range but, instead, may show a stronger relation with higher frequencies, as shown in Fig. S4. Furthermore, in both β and γ, the distribution of the preferential firing phases revealed that significantly modulated FS cells fired earlier than the RS cells ($P = 0.01$, two-sample permutation test; Fig. 3*C*).

Large-Scale Coherence of Local Field Activities and Units During β and γ. Correlations during β- and γ-oscillations represented as a function of distance displayed marked differences between awake, REM, and SWS (Fig. 4*A*). During SWS, fast oscillations displayed a remarkable spatiotemporal coherence, as indicated by the high values of spatial correlations for large distances, in contrast to the steeper decline of spatial correlations with distance during waking and REM. Although the strong links of spatial correlations were present during both wakefulness and SWS, large patterns of strong links can mostly be seen during SWS (Figs. S5 and S6). The stronger correlation during SWS is further confirmed by the correlation between spikes and LFPs as a function of distance (Fig. 4*B*). This analysis shows that during SWS, only FS cells expressed a high degree of significant phase-locking with fast-field oscillations over large cortical distances (up to 3 mm). In contrast, during wakefulness, attempts to find correlations between the β/γ recorded by one electrode and units recorded by other electrodes were unsuccessful. Finally, considering that some cells show large-scale correlations of their firing with LFPs, we also tested whether they show spike synchrony with each other during β/γ-oscillations. During SWS high-frequency oscillations, only FS cells show statistically significant

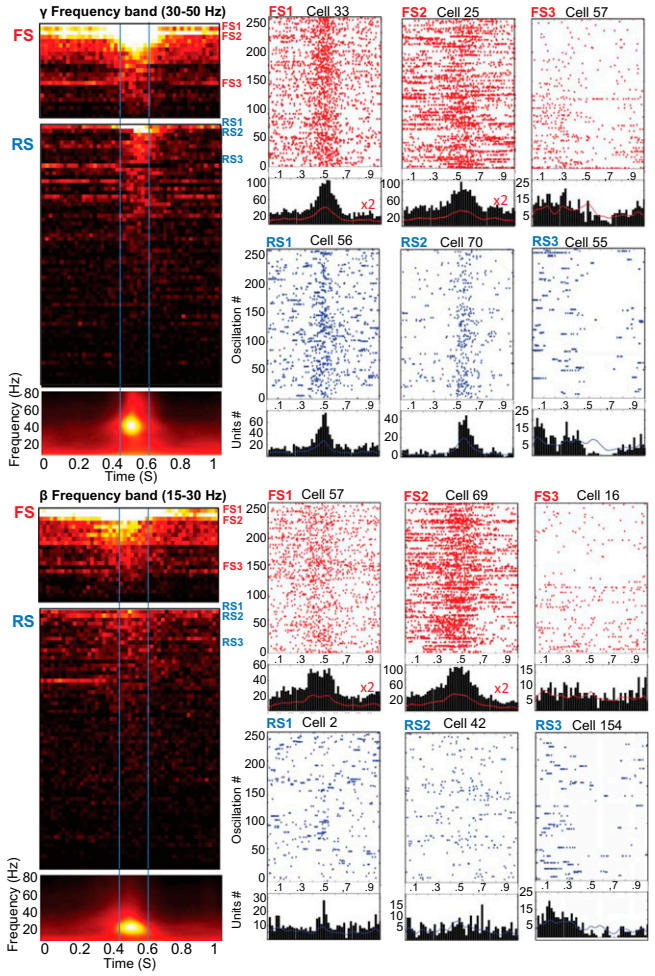

Fig. 2. Oscillation-triggered probability density of firing rates for RS and FS neurons. In each triplet set of heat maps, one shows wavelet time frequency (*Bottom*) and the other two show FS (*Top*) and RS (*Middle*) firing during these example γ- and β-oscillations. The firing rate is color-coded [black, baseline firing rate; white, 5 standard deviations (std) from the baseline]. The cells are ordered by their discharge probability during γ- or β-oscillation (20-ms bin size). A large proportion of FS cells show an increased firing rate during γ and β. Raster plots show spiking patterns of a few sample FS and RS cells. In these raster plots, each row is the spiking of the example cell in one (γ or β) oscillatory epoch. The corresponding average firing pattern (rows in the heat map) for each example cell (FS1, RS2, etc.) is indicated along the right edge of the heat maps. Note the remarkably heterogeneous discharge patterns.

spike synchrony with other FS cells (Fig. 4*C*). Additionally, these strong correlations did not show any distance dependence. A given cell (such as cell 57 or 69 in the example shown in Fig. 4*D*) may show strong synchrony (during oscillatory events) with cells that are distant within the same recording multielectrode array. This synchronous spiking could even extend to other cells recorded in another cortical area (from PMd to M1). By contrast, no such correlations over large distances were present for periods of waking.

Oscillatory Wave Propagation. LFPs recorded across the multielectrode arrays showed patterns of traveling waves in both β- and γ-oscillatory events during wakefulness, SWS, and REM (Fig. 5). These oscillatory traveling waves exhibited speeds of ~500 mm·s^{-1} and showed repeated stereotypical spatiotemporal patterns within a given multielectrode array. Such stereotypical behavior could be reminiscent of an underlying connectivity and/or barrage of directed input and outputs. The relative phase difference of each LFP compared with the global mean, averaged over all detected oscillations, revealed the spatial dynamics of dominant propagating wave directions (Fig. 5 *A2* and *A4*). A phase-based approach to detect individual traveling waves identified events with some heterogeneity (*Materials and Methods* and Movies S1–S3) that generally follow the dominant direction. Both β- and γ-oscillatory events exhibited similar distributions of phase speed, whereas δ-frequency events exhibited speeds lower by almost an order of magnitude (Fig. 5*B*, *Left*). Identified γ-frequency wave events exhibited similar phase speed distributions across wakefulness, SWS, and REM (Fig. 5*B*, *Right*), indicating possibly similar mechanisms for this wave-like behavior across the functional states of the network.

Discussion

Sleep studies of neocortical β- and γ-rhythms have been mostly focused on their macroscopic manifestation and grouping of different rhythms (23–26). It has been shown that coherent γ-oscillations are present during REM in magnetoencephalography (MEG) recordings (10). Evidence from extracranial EEG and iEEG recordings in epileptics shows that the synchrony of macroscopic γ is lower in SWS and REM relative to the awake state (27) and that γ-presence shows a phasic expression during SWS (11, 28). In this study, we took advantage of high spatial sampling of 10 × 10 multielectrode arrays in humans and monkeys, and further confirmed that β and γ are prominently present during the sleep–wake cycle at the level of neocortical microcircuitry (Fig. 1). Our findings show that the transient fast rhythms in wake-sleep are not limited to allocortex and that β and γ are preserved across different neocortical areas (e.g., temporal, premotor, motor

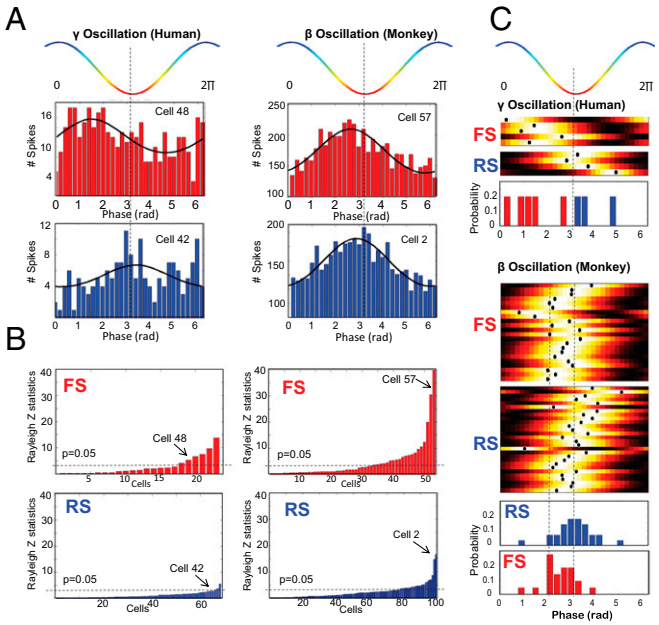

Fig. 3. Phase-locking of spikes relative to the field oscillation cycle for RS and FS neurons during SWS. Phase-locking was considered significant if the hypothesis of circular uniformity for its field phase distribution could be rejected at $P = 0.05$ using a Rayleigh statistical test. (*A*) Phase distributions of several significantly phase-locked RS and FS cells. The distributions were fitted with a von Mises function depicted here with continuous black lines. rad, radian. (*B*) Histogram of Rayleigh's *Z* value for all investigated RS (blue) and FS (red) cells. Note the large proportion of FS cells that were modulated by β and γ patterns. (*C*) Histograms of preferred firing phase for significantly phase-locked neurons. For each RS (blue) and FS (red) cell, the normalized distribution is depicted (hot colors), with black dots indicating the preferred firing phase. Note that, on average, FS cells fired earlier than RS cells.

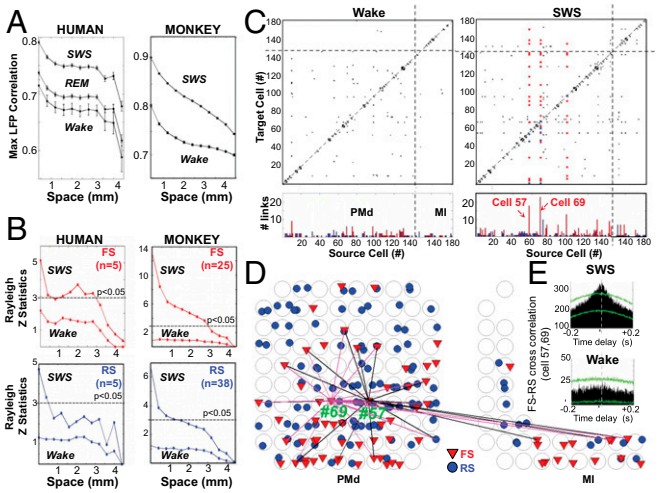

Fig. 4. Large-scale coherence of LFP activities and spikes during wake-sleep γ- and β-oscillations. (*A*) Field–field correlations: maximum (Max) of the cross-correlation (within a time lag ranging from −50 to 50 ms) averaged over all filtered LFPs (in the γ-frequency range for human and in the β-frequency range for monkey) vs. spatial distance. In both human and monkey, fast oscillations displayed locally correlated dynamics in all states, but the correlations decline with distance. During SWS, correlations stayed high across cortical distances of several millimeters. (*B*) Spike-field correlations: averaged Rayleigh's *Z* value vs. distance from LFP sites for all significantly locked RS and FS neurons. During SWS, FS neurons are phase-locked with a field over up to 3 mm in both human and monkey. This phase-locking disappears during wakefulness. In contrast, RS neurons show less spatial coherence during SWS and no significant correlation with distant LFP sites during wakefulness. (*C*) Cell–cell correlations: matrices of significant spike synchronization for PMd and MI cells during β-oscillations in monkey. For SWS, the type of target cells is indicated for cells 57/69 with colors (red, FS; and blue, RS). Note that most of the cell–cell interactions over the extent of the array are FS. (*D*) Spatial distribution of significant cell–cell interactions for two FS cells. Spike synchrony with cell 57/69 can be seen with cells that are spatially far apart. This synchronous spiking could even extend to other cells recorded in another cortical area (from PMd to M1). (*E*) Example of spike cross-correlogram during SWS and Wake states. Note the presence of a significant peak around zero during SWS that disappears during the Wake state (in green, mean ± 3 SDs of 100 surrogates generated by temporal jittering).

studied here). Additionally, we observed a clear heterogeneity of firing patterns in both cell populations during both β and γ (Fig. 2). Our results show that the cellular correlates of β- and γ-oscillations implicate both inhibitory and excitatory populations, but with a clear prominence of inhibitory cells.

Theoretically, it has been shown that inhibition plays a dominant role in generating synchrony (29), and is implicated in the large-scale synchronization of oscillations in the thalamocortical system (30). Experimental evidence also points to a more effective γ-elicitation through optogenetic stimulation of inhibitory, rather than excitatory, cells (31). Regardless, it is still controversial as to whether fast rhythms, such as γ, are generated through an exclusive interaction between interneurons [interneuron gamma (ING)] or via pyramidal-interneuron gamma (PING). A detailed account of fast oscillation's cellular mechanisms is provided elsewhere (32–34). However, the big picture is fairly intricate and involves an array of complex cellular and subcellular mechanisms (22, 33). Nonetheless, although extracellular recordings cannot directly discern mechanisms such as ING vs. PING, they can provide a channel to study patterns of ensemble activity during fast rhythms. We observed that even though both inhibitory FS and excitatory RS cells are implicated in β- and γ-oscillatory events, a larger proportion of inhibitory cells showed higher firing (Fig. 3 *A* and *B* and Table S3). Furthermore, FS cells fired earlier than RS cells in relation to the oscillatory cycle (Fig. 3*C*). Given that prior experiments suggest cycle-by-cycle recruitment of inhibition after excitation in orchestrating high-frequency rhythms (20), it is likely that the origin of the observed fast rhythms in our experiment was either distal to the recorded region/layer or included a mixture of distal and focal elements. These possible distal contributions could be conveyed through afferents from different layers of the involved column or from neighboring areas. In fact, divergent generating mechanisms of fast rhythms, depending on the cortical layer and rhythm frequency range, have been explored previously in models and in vitro preparations (35). Even though our results show a stronger phase-locking with fast oscillations, our experimental preparation does not allow a distinction between focal and likely distal oscillation generators.

Oscillatory rhythms could coexist, manifest state-dependent variability, and act as cell assembly organizers (36, 37). Although the exact functional role of oscillations is still a matter of debate, several hypotheses propose they play a role in the representation of information; regulation of the flow of information; and, last but not least, storage and retrieval of information in neural circuitry (reviewed in ref. 38). These not mutually exclusive roles of oscillations relate rhythms to the general notion of plasticity and memory consolidation during sleep (9, 39–41). Oscillations exert these effects through coordinating population activity in local and distant neuronal assemblies in SWS (42). Different synchronization mechanisms of β and γ are thought to be related to distant interaction and local computations during cognition (43). Much emphasis of near zero-phase lag synchrony over a few millimeters has been based on awake cognitive states (44, 45), even though the initial evidence came from anesthetized state experiments (46–48). However, the synchronization of neighboring cortical sites through fast rhythms is not limited to awake or anesthetized states, and it occurs during a range of altered states of consciousness (anesthesia, SWS, and REM) (4, 49). Interestingly, we also noted that correlated firings can be detected between spatially distant (PMd and M1) FS neurons (Fig. 4).

One of the most striking observations was that the coherence of γ-oscillations markedly increases during sleep. At the level of LFPs, we found that the millimeter-scale coherence of fast oscillations is more coherent during REM sleep compared with wakefulness, in agreement with previous studies in MEG (10) and extracellular recordings in cats (6). Interestingly, this spatiotemporal coherence is even larger, and is the highest in SWS (Fig. 4 and Figs. S5 and S6). Similarly, we found that during SWS, FS cells are phase-locked with LFPs over up to 3 mm, whereas this phase-locking remains local during wakefulness. In contrast, RS cells show diminished spatial coherence during SWS and no significant correlation with distant LFP sites during wakefulness (Fig. 4). The coherence of fast oscillations during SWS, which occur focally or over a span of a few millimeters, poses a nice challenge for future modeling and experimental studies. A possible role of slow waves in memory consolidation has been well explored in the past decade (9, 50, 51). The present findings of similar fast oscillations during SWS and wakefulness are compatible with a reactivation of wake patterns. The higher coherence of SWS fast oscillations could perhaps be a substrate to induce long-term changes in cortical circuits during this reactivation. Such a possible role for fast oscillations in memory consolidation during sleep would be an interesting venue to explore.

Finally, slow oscillations show traveling waves over long distances (spanning several centimeters) during sleep (52). However, much of the information about traveling waves is based on studies in anesthetized animals (53–55). Although recent developments in multielectrode array recording technology have enabled the detection of (γ) fast oscillatory waves in anesthetized preparations (56), it is only recently that traveling β-waves have been reported in the awake state (57, 58). In a recent study, it was shown that the anisotropy of the cortical wiring may influence the spatiotemporal spike patterning (at least in the motor cortex) and that FS cells were found to fire more reliably in phase

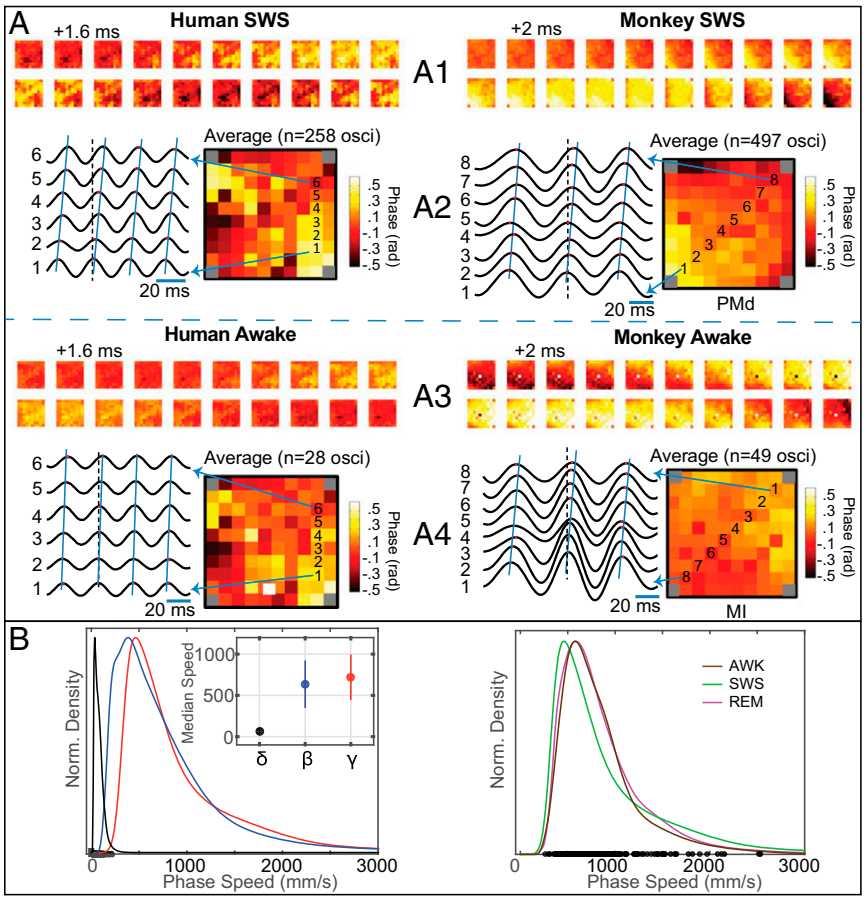

Fig. 5. (*A*) Wave propagation in the δ-frequency (0.5–4 Hz), γ-frequency (30–50 Hz), and β-frequency (15–30 Hz) ranges during SWS or wakefulness. LFPs in the γ- and β-bands from a single trial are plotted with respect to the spatial arrangement of the recording electrodes. (*A1* and *A3*) Spatiotemporal plots of example LFP waves in human γ (*Left*) and monkey β (*Right*) for both SWS (*A1*) and wakefulness (*A3*). (*A2* and *A4*) Stereotyped, repetitive spatiotemporal patterns of single oscillations (osci) were frequently observed throughout the recordings. (*B*) Phase speed distributions across frequency bands and across network states in human. (*Left*) Plotted are the kernel smoothing density estimates for δ-, β-, and γ-frequency bands during SWS. Speed estimates from individual δ-epochs are plotted on the abscissa (black dots). Propagation in the δ-frequency band exhibited speeds predominantly in the 10–100 mm·s^{-1} range, whereas β- and γ-frequency propagation exhibited higher speeds (*Inset*; median + median absolute deviation). (*Right*) γ-Oscillations across different states exhibited similar distributions of propagation speed. Speed estimates from individual γ-epochs in the awake state are plotted on the abscissa (black dots). AWK, awake; Norm., normalized.

with the β-oscillation (59). In the present paper, we adapted a phase-based method (60) to detect propagating fast oscillatory waves, and found that both wakefulness and sleep harbor these waves (Fig. 5) and that their speed is not affected by the state of consciousness. However, they do exhibit a tendency to manifest stereotypical directionality (Fig. 5 and Movies S1–S3). Dominant directionality could be related to the underlying connectivity profile that serves the intra- and intercortical information transfer (57). The computational implication of horizontal connections could point to a preset preferred path for information processing within a given functional domain of the neocortex (60–62). That such a directional path is "functionally" preserved in sleep could be further evidence that corticothalamic UP states replay fragments of wakefulness (63). The fast oscillations dynamics that we found here are consistent with such reactivation.

Conclusion

These findings confirm and extend earlier studies reporting high-frequency oscillations (>20 Hz) during sleep (4, 6, 11). In particular, we found that β- and γ-oscillations organize and modulate cortical population activity during SWS in the form of coherent waves traveling over several millimeters in the human/monkey neocortex. In addition, we observed that FS cells are strongly involved in the generation of these spatiotemporal patterns. The partial overlap between the spatial distribution of β/γ-oscillations during sleep and wakefulness (57) suggests that these waves share similar functional attributes. During sleep, they may replay wake patterns with increased coherence that could play a role in memory consolidation.

Materials and Methods

In epileptic humans with intractable seizures, 10 × 10 multielectrode arrays (400-μm interelectrode separation, 1.0-mm electrode length) were implanted in the middle temporal gyrus. Patients consented to the procedure, which was approved by the Massachusetts General Hospital's Institutional Review Board in accordance with the ethical standards of the Declaration of Helsinki. In monkeys, similar arrays were implanted in the MI and PMd. The procedure was approved by the University of Chicago's Institutional Animal Care and Use Committee and conformed to the principles outlined in the Guide for the Care and Use of Laboratory Animals (64). Details of cell categorization, β- and γ-event detection, synchrony, and analysis of spatiotemporal activity patterns are provided elsewhere (11–13, 60, 65–67) and in *Supporting Information*.

ACKNOWLEDGMENTS. We thank Zach Haga for monkey data collection. Research was funded by Harvard's Wyss Institute for Biologically Inspired Engineering; Agence Nationale de le Recherche ANR-10-IAIHU-06; the CNSR European Community Future and Emerging Technologies program (BrainScales FP7-269921 and The Human Brain Project FP7-604102); the ONR (Multidisciplinary University Research Initiatives Award N00014-13-1-0672); and NIH Grants 5R01NS062092, R01EB009282, R01NS045853, and R01MH099645. L.E.M. was supported by NIH Training Grant 5T32EY20503-5.

1. Brovelli A, et al. (2004) Beta oscillations in a large-scale sensorimotor cortical network: Directional influences revealed by Granger causality. *Proc Natl Acad Sci USA* 101(26): 9849–9854.
2. Donoghue JP, Sanes JN, Hatsopoulos NG, Gaál G (1998) Neural discharge and local field potential oscillations in primate motor cortex during voluntary movements. *J Neurophysiol* 79(1):159–173.
3. Fries P, Nikolić D, Singer W (2007) The gamma cycle. *Trends Neurosci* 30(7):309–316.
4. Steriade M, Amzica F, Contreras D (1996) Synchronization of fast (30-40 Hz) spontaneous cortical rhythms during brain activation. *J Neurosci* 16(1):392–417.
5. Steriade M, McCarley RW (2005) *Brainstem Control of Wakefulness and Sleep* (Kluwer Academic, New York).
6. Destexhe A, Contreras D, Steriade M (1999) Spatiotemporal analysis of local field potentials and unit discharges in cat cerebral cortex during natural wake and sleep states. *J Neurosci* 19(11):4595–4608.
7. Clemens Z, et al. (2007) Temporal coupling of parahippocampal ripples, sleep spindles and slow oscillations in humans. *Brain* 130(Pt 11):2868–2878.
8. Buzsáki G (1998) Memory consolidation during sleep: A neurophysiological perspective. *J Sleep Res* 7(Suppl 1):17–23.
9. Diekelmann S, Born J (2010) The memory function of sleep. *Nat Rev Neurosci* 11(2): 114–126.
10. Llinás R, Ribary U (1993) Coherent 40-Hz oscillation characterizes dream state in humans. *Proc Natl Acad Sci USA* 90(5):2078–2081.
11. Le Van Quyen M, et al. (2010) Large-scale microelectrode recordings of high-frequency gamma oscillations in human cortex during sleep. *J Neurosci* 30(23):7770–7782.
12. Peyrache A, et al. (2012) Spatiotemporal dynamics of neocortical excitation and inhibition during human sleep. *Proc Natl Acad Sci USA* 109(5):1731–1736.
13. Dehghani N, et al. (2016) Dynamic balance of excitation and inhibition in human and monkey neocortex. *Sci Rep* 6:23176.
14. Bazhenov M, Timofeev I (2006) Thalamocortical oscillations. *Scholarpedia* 1(6):1319.
15. Haider B, Duque A, Hasenstaub AR, McCormick DA (2006) Neocortical network activity in vivo is generated through a dynamic balance of excitation and inhibition. *J Neurosci* 26(17):4535–4545.
16. Csicsvari J, Jamieson B, Wise KD, Buzsáki G (2003) Mechanisms of gamma oscillations in the hippocampus of the behaving rat. *Neuron* 37(2):311–322.
17. Hájos N, et al. (2004) Spike timing of distinct types of GABAergic interneuron during hippocampal gamma oscillations in vitro. *J Neurosci* 24(41):9127–9137.
18. Sohal VS, Huguenard JR (2005) Inhibitory coupling specifically generates emergent gamma oscillations in diverse cell types. *Proc Natl Acad Sci USA* 102(51):18638–18643.
19. Quilichini P, Sirota A, Buzsáki G (2010) Intrinsic circuit organization and theta-gamma oscillation dynamics in the entorhinal cortex of the rat. *J Neurosci* 30(33):11128–11142.
20. Atallah BV, Scanziani M (2009) Instantaneous modulation of gamma oscillation frequency by balancing excitation with inhibition. *Neuron* 62(4):566–577.
21. Whittington MA, Traub RD, Kopell N, Ermentrout B, Buhl EH (2000) Inhibition-based rhythms: Experimental and mathematical observations on network dynamics. *Int J Psychophysiol* 38(3):315–336.
22. Traub RD, Whittington MA, Jefferys JG (1999) *Fast Oscillations in Cortical Circuits* (MIT Press, Cambridge, MA).
23. Buchsbaum MS, et al. (1982) Topographic cortical mapping of EEG sleep stages during daytime naps in normal subjects. *Sleep* 5(3):248–255.
24. Steriade M (2006) Grouping of brain rhythms in corticothalamic systems. *Neuroscience* 137(4):1087–1106.
25. Ayoub A, Mölle M, Preissl H, Born J (2012) Grouping of MEG gamma oscillations by EEG sleep spindles. *Neuroimage* 59(2):1491–1500.
26. Valencia M, Artieda J, Bolam JP, Mena-Segovia J (2013) Dynamic interaction of spindles and gamma activity during cortical slow oscillations and its modulation by subcortical afferents. *PLoS One* 8(7):e67540.
27. Cantero JL, Atienza M, Madsen JR, Stickgold R (2004) Gamma EEG dynamics in neocortex and hippocampus during human wakefulness and sleep. *Neuroimage* 22(3): 1271–1280.
28. Valderrama M, et al. (2012) Human gamma oscillations during slow wave sleep. *PLoS One* 7(4):e33477.
29. Van Vreeswijk C, Abbott LF, Ermentrout GB (1994) When inhibition not excitation synchronizes neural firing. *J Comput Neurosci* 1(4):313–321.
30. Destexhe A, Contreras D, Steriade M (1998) Mechanisms underlying the synchronizing action of corticothalamic feedback through inhibition of thalamic relay cells. *J Neurophysiol* 79(2):999–1016.
31. Cardin JA, et al. (2009) Driving fast-spiking cells induces gamma rhythm and controls sensory responses. *Nature* 459(7247):663–667.
32. Buzsáki G, Wang XJ (2012) Mechanisms of gamma oscillations. *Annu Rev Neurosci* 35: 203–225.
33. Traub RD (2006) Fast oscillations. *Scholarpedia* 1(12):1764.
34. Tiesinga P, Sejnowski TJ (2009) Cortical enlightenment: Are attentional gamma oscillations driven by ING or PING? *Neuron* 63(6):727–732.
35. Roopun AK, et al. (2006) A beta2-frequency (20-30 Hz) oscillation in nonsynaptic networks of somatosensory cortex. *Proc Natl Acad Sci USA* 103(42):15646–15650.
36. Buzsáki G, Draguhn A (2004) Neuronal oscillations in cortical networks. *Science* 304(5679):1926–1929.
37. Buzsáki G (2006) *Rhythms of the Brain* (Oxford Univ Press, New York).
38. Sejnowski TJ, Paulsen O (2006) Network oscillations: Emerging computational principles. *J Neurosci* 26(6):1673–1676.
39. Maquet P (2001) The role of sleep in learning and memory. *Science* 294(5544): 1048–1052.
40. Sejnowski TJ, Destexhe A (2000) Why do we sleep? *Brain Res* 886(1-2):208–223.
41. Steriade M, Timofeev I (2003) Neuronal plasticity in thalamocortical networks during sleep and waking oscillations. *Neuron* 37(4):563–576.
42. Crunelli V, Hughes SW (2010) The slow (<1 Hz) rhythm of non-REM sleep: A dialogue between three cardinal oscillators. *Nat Neurosci* 13(1):9–17.
43. Kopell N, Ermentrout GB, Whittington MA, Traub RD (2000) Gamma rhythms and beta rhythms have different synchronization properties. *Proc Natl Acad Sci USA* 97(4): 1867–1872.
44. Kreiter AK, Singer W (1992) Oscillatory neuronal responses in the visual cortex of the awake macaque monkey. *Eur J Neurosci* 4(4):369–375.
45. Murthy VN, Fetz EE (1996) Synchronization of neurons during local field potential oscillations in sensorimotor cortex of awake monkeys. *J Neurophysiol* 76(6): 3968–3982.
46. Eckhorn R, et al. (1988) Coherent oscillations: A mechanism of feature linking in the visual cortex? Multiple electrode and correlation analyses in the cat. *Biol Cybern* 60(2):121–130.
47. Engel AK, Kreiter AK, König P, Singer W (1991) Synchronization of oscillatory neuronal responses between striate and extrastriate visual cortical areas of the cat. *Proc Natl Acad Sci USA* 88(14):6048–6052.
48. Gray CM, König P, Engel AK, Singer W (1989) Oscillatory responses in cat visual cortex exhibit inter-columnar synchronization which reflects global stimulus properties. *Nature* 338(6213):334–337.
49. Steriade M, Contreras D, Amzica F, Timofeev I (1996) Synchronization of fast (30-40 Hz) spontaneous oscillations in intrathalamic and thalamocortical networks. *J Neurosci* 16(8):2788–2808.
50. Mölle M, Marshall L, Gais S, Born J (2004) Learning increases human electroencephalographic coherence during subsequent slow sleep oscillations. *Proc Natl Acad Sci USA* 101(38):13963–13968.
51. Marshall L, Helgadóttir H, Mölle M, Born J (2006) Boosting slow oscillations during sleep potentiates memory. *Nature* 444(7119):610–613.
52. Massimini M, Huber R, Ferrarelli F, Hill S, Tononi G (2004) The sleep slow oscillation as a traveling wave. *J Neurosci* 24(31):6862–6870.
53. Bringuier V, Chavane F, Glaeser L, Frégnac Y (1999) Horizontal propagation of visual activity in the synaptic integration field of area 17 neurons. *Science* 283(5402): 695–699.
54. Grinvald A, Lieke EE, Frostig RD, Hildesheim R (1994) Cortical point-spread function and long-range lateral interactions revealed by real-time optical imaging of macaque monkey primary visual cortex. *J Neurosci* 14(5 Pt 1):2545–2568.
55. Xu W, Huang X, Takagaki K, Wu JY (2007) Compression and reflection of visually evoked cortical waves. *Neuron* 55(1):119–129.
56. Gabriel A, Eckhorn R (2003) A multi-channel correlation method detects traveling gamma-waves in monkey visual cortex. *J Neurosci Methods* 131(1-2):171–184.
57. Rubino D, Robbins KA, Hatsopoulos NG (2006) Propagating waves mediate information transfer in the motor cortex. *Nat Neurosci* 9(12):1549–1557.
58. Takahashi K, Saleh M, Penn RD, Hatsopoulos NG (2011) Propagating waves in human motor cortex. *Front Hum Neurosci* 5(40):40.
59. Takahashi K, et al. (2015) Large-scale spatiotemporal spike patterning consistent with wave propagation in motor cortex. *Nat Commun* 6:7169.
60. Muller L, Reynaud A, Chavane F, Destexhe A (2014) The stimulus-evoked population response in visual cortex of awake monkey is a propagating wave. *Nat Commun* 5:3675.
61. Gilbert CD (1992) Horizontal integration and cortical dynamics. *Neuron* 9(1):1–13.
62. Ermentrout GB, Kleinfeld D (2001) Traveling electrical waves in cortex: Insights from phase dynamics and speculation on a computational role. *Neuron* 29(1):33–44.
63. Destexhe A, Hughes SW, Rudolph M, Crunelli V (2007) Are corticothalamic 'up' states fragments of wakefulness? *Trends Neurosci* 30(7):334–342.
64. NIH (1985) *Guide for the Care and Use of Laboratory Animals* (Natl Inst Health, Bethesda), DHHS Publ. No. (NIH) 86-23.
65. Hatsopoulos NG, Geman S, Amarasingham A, Bienenstock E (2003) At what time scale does the nervous system operate? *Neurocomputing* 52-54:25–29.
66. Le Van Quyen M, Bragin A (2007) Analysis of dynamic brain oscillations: methodological advances. *Trends Neurosci* 30(7):365–373.
67. Dehghani N, et al. (2012) Avalanche analysis from multielectrode ensemble recordings in cat monkey, and human cerebral cortex during wakefulness and sleep. *Front Physiol* 3(302):302.
68. Raos V, Franchi G, Gallese V, Fogassi L (2003) Somatotopic organization of the lateral part of area F2 (dorsal premotor cortex) of the macaque monkey. *J Neurophysiol* 89(3):1503–1518.
69. Kalaska JF, Cohen DA, Hyde ML, Prud'homme M (1989) A comparison of movement direction-related versus load direction-related activity in primate motor cortex, using a two-dimensional reaching task. *J Neurosci* 9(6):2080–2102.
70. Jacobs J, Kahana MJ, Ekstrom AD, Fried I (2007) Brain oscillations control timing of single-neuron activity in humans. *J Neurosci* 27(14):3839–3844.
71. de la Rocha J, Doiron B, Shea-Brown E, Josić K, Reyes A (2007) Correlation between neural spike trains increases with firing rate. *Nature* 448(7155):802–806.

Supporting Information

Le Van Quyen et al. 10.1073/pnas.1523583113

Recordings

In two epileptic humans with intractable seizures, 10 × 10 Neuroprobe silicon multielectrode arrays (Blackrock Microsystems) were implanted in the middle temporal gyrus. In both patients, the histological examination of the implanted tissue in the therapeutic resection related the recording locations to neocortical layers II/III. Continuous recordings in the epilepsy monitoring unit were used for this study (48 h for two nights for patient 1, and 24 h for one night for patient 2). Electrodes were implanted in regions expected to be removed, and after the monitoring session, the implant area was excised. Patients consented to the procedure, which was approved by the Massachusetts General Hospital Institutional Review Board in accordance with the ethical standards of the Declaration of Helsinki. In the monkey, similar arrays (UTAH array, 400-μm interelectrode separation, 1.0-mm electrode length; BlackRock Microsystems) were implanted in MI and PMd. Ninety-six electrodes in PMd and 32 electrodes in MI were recorded. Based on histological analysis of PMd (68), a depth of 1 mm from the pial surface is likely to target deep portions of layers II/III. Based on histological analysis of MI (69), a depth of 1 mm from the pial surface in MI targets layers II/III. Data were recorded continuously each night for two nights in a row; awake data were collected in the day between these nights. The procedure was approved by the University of Chicago's Institutional Animal Care and Use Committee and conformed to the principles outlined in the *Guide for the Care and Use of Laboratory Animals* (64). Additional details on procedures are provided by Dehghani et al. (67).

Patients

Patient 1 was a 52-y-old, right-handed woman at the time of a continuous 8-d phase II video-invasive EEG monitoring study. The patient had a history of complex partial seizures with occasional secondary generalization, beginning at the age of 4 y, and she typically suffered from 10–15 events per day. Her seizures usually presented with sudden speech arrest associated with confusion and repetition of activities. MRI showed a region of encephalomalacia in the left temporooccipital region. The NeuroPort microelectrode array was placed in the middle temporal gyrus. The distance to the nearest electrocorticogram (ECoG) electrode where seizure onsets were detected was ∼2 cm. At the conclusion of the study, the patient underwent resection of the left anterior temporal lobe. Pathology showed hippocampal sclerosis with secondary cortical gliosis but not in the region around the microelectrode array. The patient remained seizure-free for 1 y after the resection, but seizures returned after this period.

Patient 2 was a 24-y-old, right-handed woman at the time of a continuous 4-d phase II video-invasive EEG monitoring study. Her seizures tended to present with staring spells, gulping sounds, a general feeling of heat, and hand automatisms, which began around the age of 14 y. EEG monitoring from a phase I study suggested that these seizures originated from the left anterior temporal region. MRI showed a large lesion in the left temporal lobe, believed to be a glioma. In accordance with the above findings, the patient was implanted with a combination of subdural and depth electrodes focused on the left temporal region. The NeuroPort research electrode was placed in the middle temporal gyrus about 2 cm posterior to the temporal tip. The distance to the nearest ECoG electrode where seizure onsets were detected was ∼4 cm. At the conclusion of the study, the patient underwent a left anterior temporal lobectomy, a left amygdalohippocampectomy, and a lesionectomy of the posterior temporal lobe. Pathology determined the lesion to be a low-grade glioneuronal tumor, although by MRI and histology, the cortex underlying the microelectrode array did not appear abnormal. At last evaluation, 6 mo postoperatively, the patient was seizure-free.

Spike Sorting and Cell Categorization

After offline spike sorting based on principal component analysis, each cell's average spike waveforms were used to extract the half-width of the extracellular positive deflection and the valley-to-peak parameter. Using a K-means algorithm, these average waveforms were further clustered into two distinct groups. Cross-correlation between cell pairs was used to detect interactions indicative of putative monosynaptic connections. This combined morpho-functional characterization of cells was used to categorize them as putative excitatory (RS) and putative inhibitory (FS) cells. Rigorous multivariable quantification and clustering were implemented to obtain robust cell categorization. Only the robustly categorized cells were included in the analyses (patient 1, 68 RS and 23 FS neurons; patient 2, 30 RS and 5 FS neurons; monkey, 99 RS and 53 FS neurons). More details are provided in the supporting information of Peyrache et al. (12) and Dehghani et al. (13).

Automatic Detection of High-Frequency Oscillation and Time-Frequency Decomposition

The Hilbert transform was used to extract the envelope of the filtered LFPs from 15–30 Hz and 30–50 Hz for β and γ, respectively. Oscillatory events were detected as significant deviations of the envelope average over the 96-electrode array in these specified frequency ranges. These events had to be longer than a minimal duration (i.e., 75 ms for γ-oscillations). The amplitude of these oscillatory events had to pass the mean envelope ± 2 SDs in the corresponding frequency band over the entire period of recording. The oscillatory events were visually confirmed and included in the analyses only if they did not contain any epileptic activity (in humans). The Morlet wavelet was used for time-frequency decomposition and precise characterization of the mean frequency, beginning, maximum amplitude, and onset and offset of each oscillation (66). These timing features were used for calculation of average time-frequency representations; for details see ref. 11.

Spike and LFP Phase-Locking

The Morlet wavelet was used to calculate the power and oscillatory phase of the frequency ranges of β and γ. A neuron was considered phase-locked to a given fast oscillation band if the hypothesis of its LFP phase distribution circular uniformity was rejected (at $P < 0.05$) based on a Bonferroni-corrected Rayleigh test. See refs. 11 and 70 for the detailed methodology.

Spike Synchrony

For creating surrogate data, every spike (in a given spike series of a cell) was jittered. The value of jittering was randomly and independently selected from a uniform distribution between −100 and 100 ms. Realization of this procedure for 100 times provided the statistical basis ($P = 0.01$) for 99% confidence intervals in each bin. If the cross-correlogram surpassed this surrogate statistical threshold, coincident spiking was considered synchronous; for more details see ref. 65. Furthermore, in analysis of surrogate data, we used a large jitter window of 100 ms. Our results indicated that correlograms were not sensitive to the size of this window within a broad range (25–100 ms). Finally, to avoid spurious detections associated with brief bursts of spikes, we compared measurements of correlation with measurements of correlation normalized by the geometric mean of each cell

pair's average firing rates (71). Similar results were obtained, suggesting that our observations did not simply reflect the synchrony generated by bursts of activities.

Spatiotemporal Dynamics

As in previous work (57, 60), LFPs filtered in the frequency ranges for β and γ (eighth-order Butterworth, forward-reverse in time) were transformed into a complex time series via the analytic signal representation. Detection of oscillatory events proceeded as before (3 SDs for 100 ms). Detection of wave-like spatiotemporal organization within these oscillatory events followed an algorithmic approach modified from the phase-latency method for analysis of optical imaging data introduced by Muller et al. (60). Instantaneous speed was calculated using the methods in ref. 57.

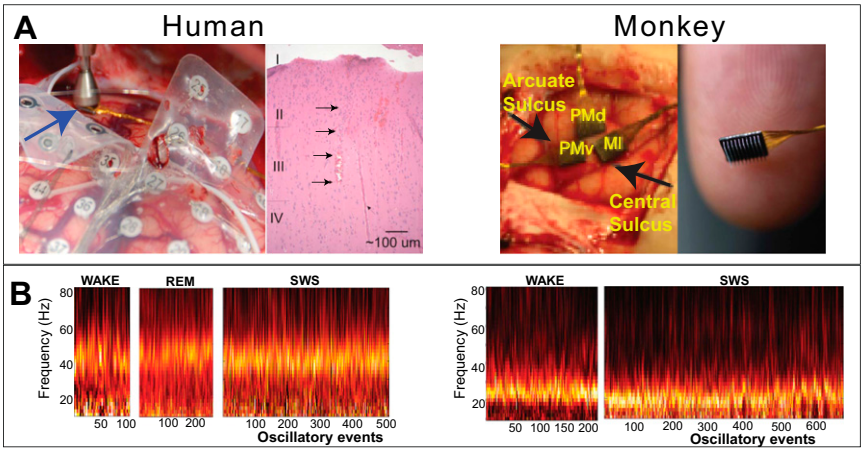

Fig. S1. γ- and β-Oscillations during sleep and wakefulness. (*A*) Recordings from (4 × 4 mm) 100-electrode Utah (Neuroprobe) arrays are shown for neocortical γ-oscillations in the temporal lobe of humans (*Left*) and β-oscillations in the PMd and MI of monkey (*Right*). (*Left*) Array is implanted using a pneumatic device (blue arrow) under an ECoG macrogrid. Histology shows that the array tract penetrates at least as far as superficial layer III (arrows). Glial fibrillary acidic protein staining highlights focal gliosis of the superficial layers of the cortex. Neuronal specific nuclear protein immunohistochemical staining reveals normal cortical layering with no evidence of cortical dysplasia. (*Right*) Sleep recordings were from PMd and MI arrays, and not a ventral premotor (PMv) array. The scale of the array is shown on the far right against the fingertip. (*B*) Power spectra of a few hundred examples of high-frequency oscillations during recorded vigilance states. Each column of the color-coded matrix is the average of time frequency during an example epoch. WAKE, wakefulness.

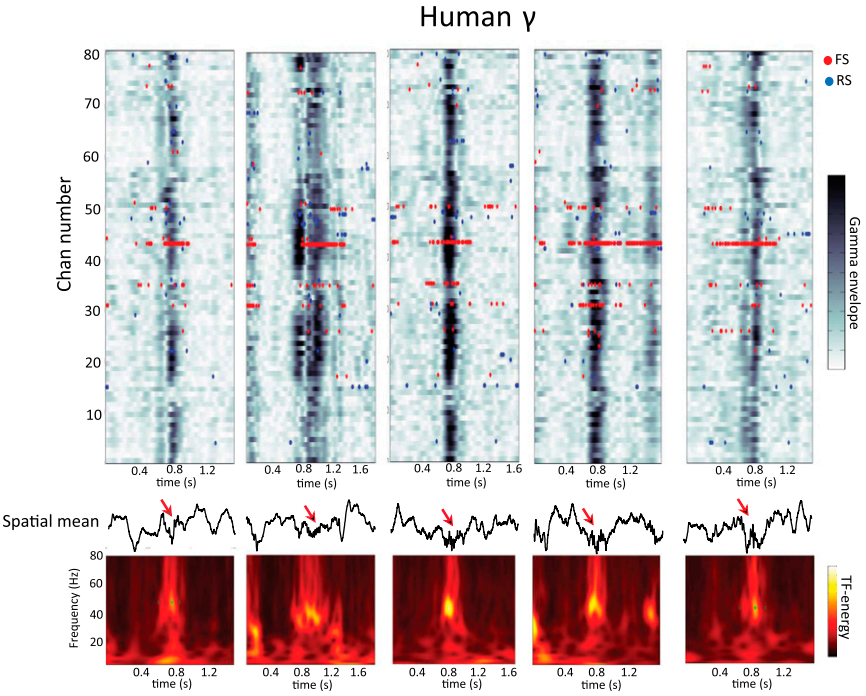

Fig. S2. Examples of neocortical γ-events in sleep. (*Top*) Example γ-events from human patient 1. In these heat maps, each row is a different LFP channel (Chan). Red and blue dots show spiking activity of FS and RS cells, localized at the same electrodes that were used to record the LFPs. (*Middle*) Raw traces of average LFP recordings. (*Bottom*) Wavelet time frequency (TF) of the average LFP.

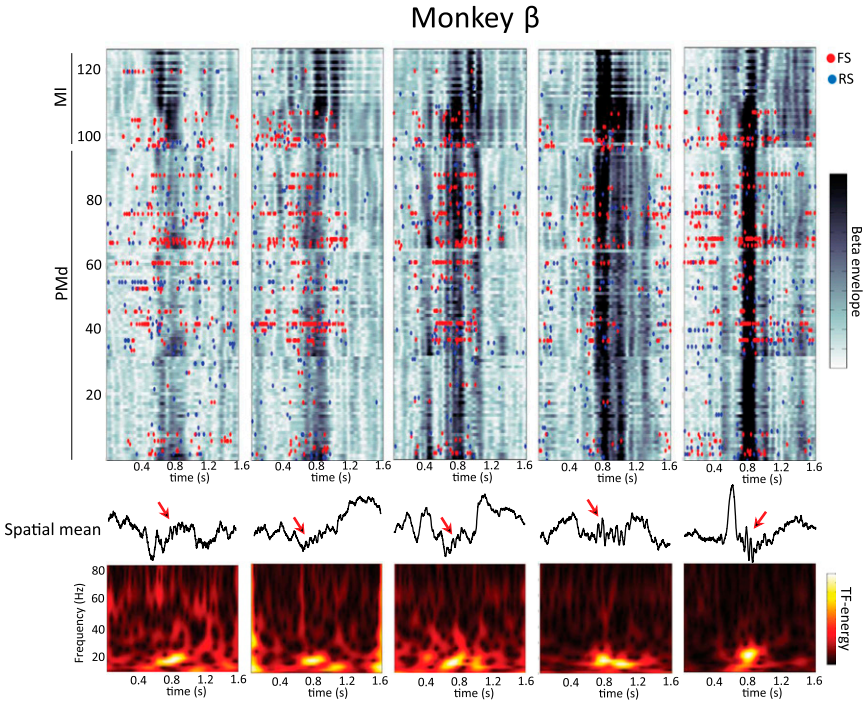

Fig. S3. Examples of neocortical β-events in sleep. (*Top*) Example β-events from monkey. In these heat maps, each row is a different LFP channel. Red and blue dots show spiking activity of FS and RS cells, localized at the same electrodes that were used to record the LFPs. (*Middle*) Raw traces of average LFP recordings. (*Bottom*) Wavelet time frequency of the average LFP.

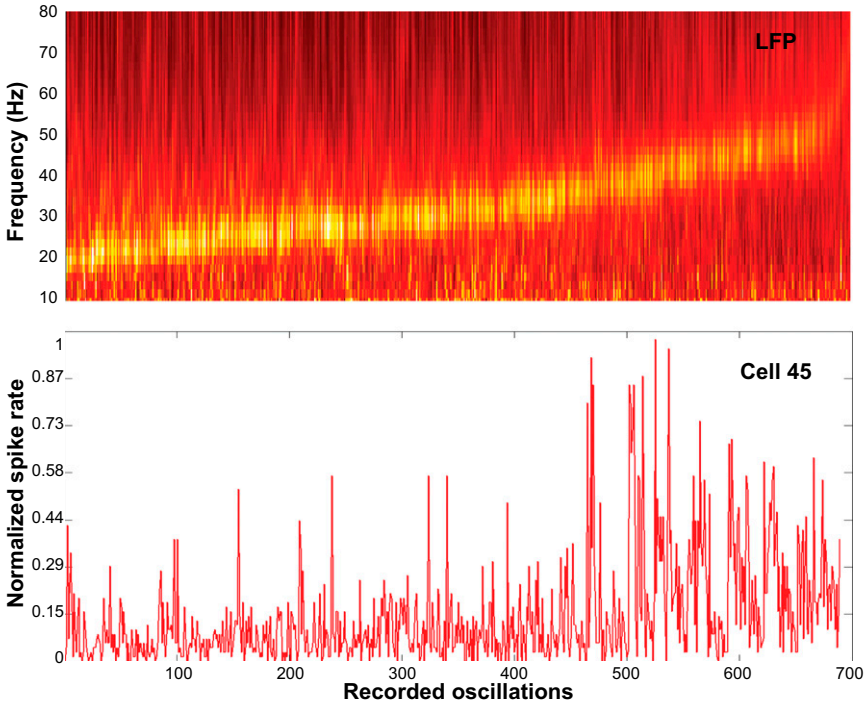

Fig. S4. Oscillation-spiking relation. In this example, ~700 oscillatory events from a given channel were studied. (*Top*) Dominant oscillating frequencies of these events were sorted from low to high (*x* axis; LFP). (*Bottom*) Corresponding normalized (to maximum) spike rate during each event of the recorded FS cell (from the same electrode). This cell shows a clear higher spiking rate relationship during higher frequencies.

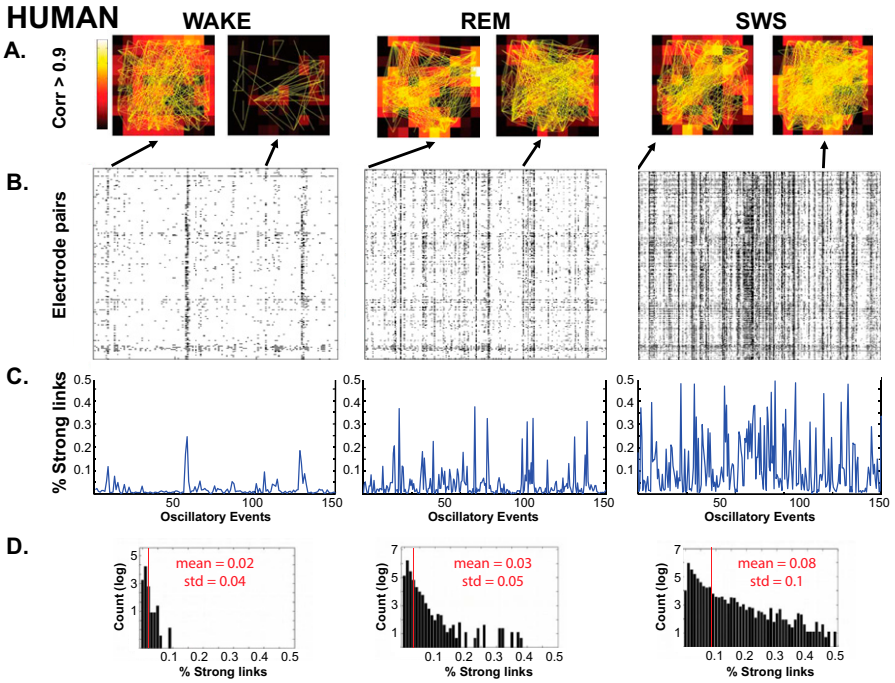

Fig. S5. (*A*) Patterns of strong links (maximum cross-correlation ≥ 0.9 over a delay of ±50 ms) occurring across the grid (human). (*B*) Patterns of pair-wise LFP spatial correlation for different states. Arrows point to the corresponding spatial profile of strong links at sample times. (*C*) Size distributions of the coherent patterns. In all states, widespread strong correlation across the grid can be seen, but they are less frequent during the WAKE state and very frequent during SWS. *C* and *D* show the percentage and statistical distribution of strong links.

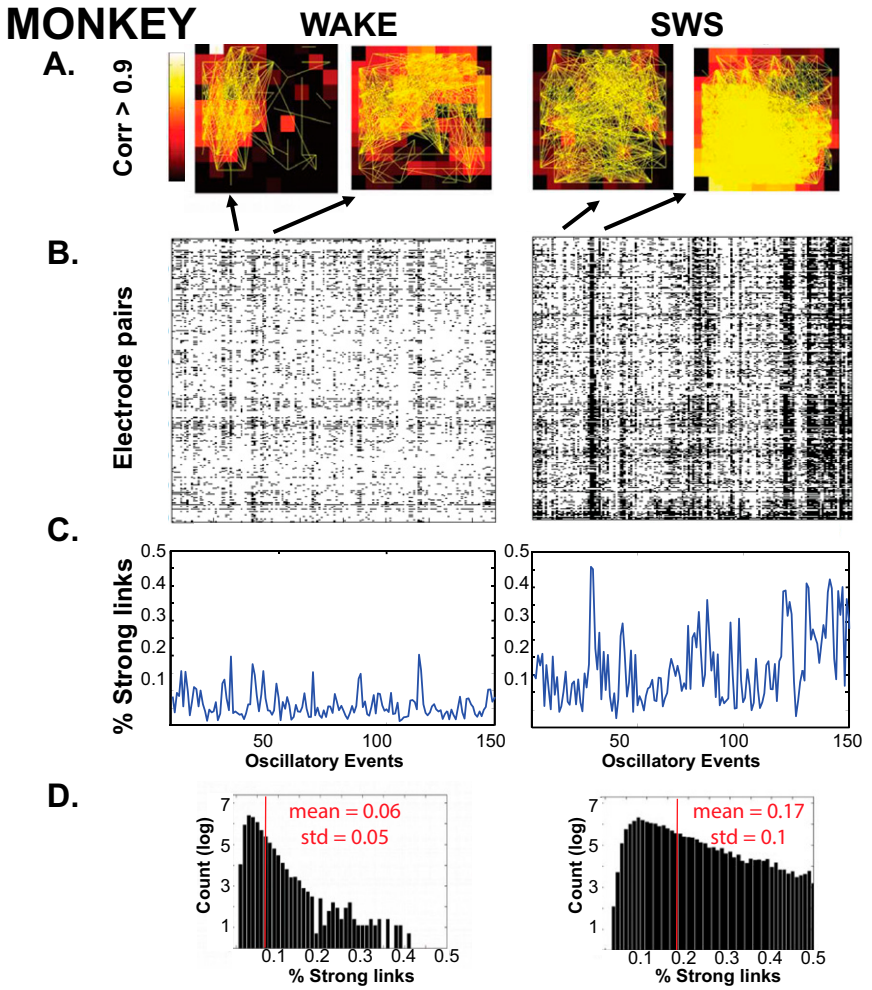

Fig. S6. (*A*) Patterns of strong links (maximum cross-correlation ≥ 0.9 over a delay of ±50 ms) occurring across the grid (Monkey). (*B*) The spatial correlations are higher during SWS than during the WAKE state. Large patterns of strong links can mostly be seen during SWS. Similar observations can be made for human data (Fig. S5). *C* and *D* show the percentage and statistical distribution of strong links.

Table S1. State-dependent oscillation amplitude

State	Mean amplitude, μV	*N*, events
Human WAKE γ	16.3 ± 9.5	188
Human REM γ	20.0 ± 16.4	1,316
Human SWS γ	30.7 ± 19.1	1,865
Monkey WAKE β	29.5 ± 11.0	3,240
Monkey SWS β	35.0 ± 17.5	8,543

For each state-oscillation category, the mean amplitude and number of events are depicted above. WAKE, wakefulness.

Table S2. State-dependent peak frequency

State	Peak frequency, Hz	Interval, s
Human WAKE γ	42.3 ± 3.8	2.4 ± 1.8
Human REM γ	41.6 ± 4.1	2.4 ± 1.8
Human SWS γ	40.9 ± 4.0	2.4 ± 1.9
Monkey WAKE β	24.6 ± 2.9	1.3 ± 0.7
Monkey SWS β	22.8 ± 3.6	1.6 ± 1.1

For each state-oscillation category, peak frequency and interepisode interval are depicted above.

Table S3. State-dependent firing rate

State	FS, Hz	RS, Hz
Human WAKE	6.4 ± 12.7 (0–57.0)	2.6 ± 3.1 (0–15.3)
Human REM	8.1 ± 8.0 (0.36–32.0)	2.1 ± 2.0 (0.03–10.4)
Human SWS	7.5 ± 9.3 (0.2–40.9)	1.9 ± 2.0 (0.03–14.1)
Monkey WAKE	9.4 ± 7.4 (0.6–31.1)	5.9 ± 4.0 (0.25–20.5)
Monkey SWS	8.7 ± 8.4 (0.5–37.6)	3.5 ± 2.6 (0.1–12.1)

For each state-cell category, the firing rate's mean, std, and range (in parentheses) are depicted.

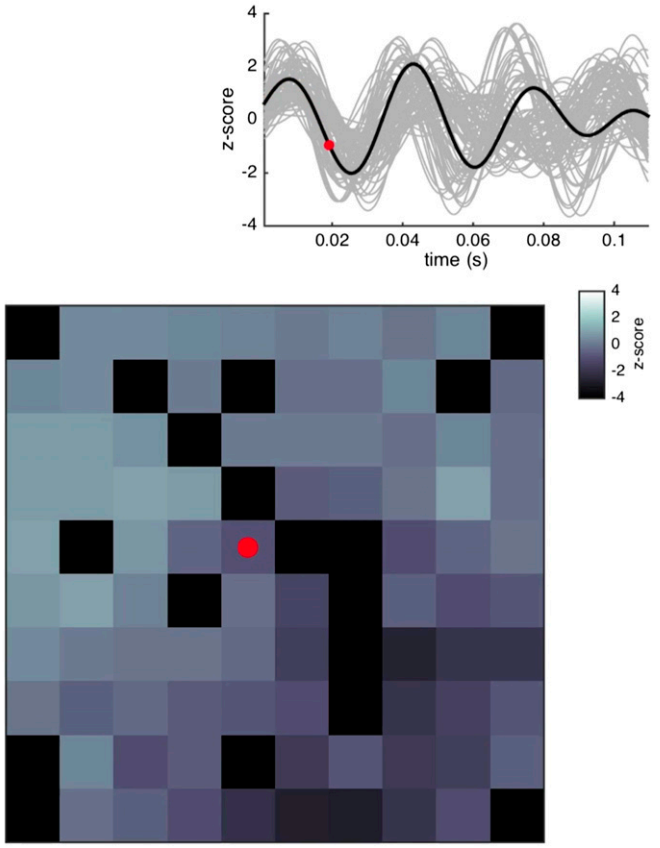

Movie S1. Spatiotemporal activity pattern in an example β-frequency wave in human SWS. In this movie, *Z*-score amplitudes are plotted in false-color (*Bottom*). In the *Top* panel, the red dot traces out the timecourse of the channel in black (shown at its corresponding array position, below); all other channels are plotted in gray.

Movie S1

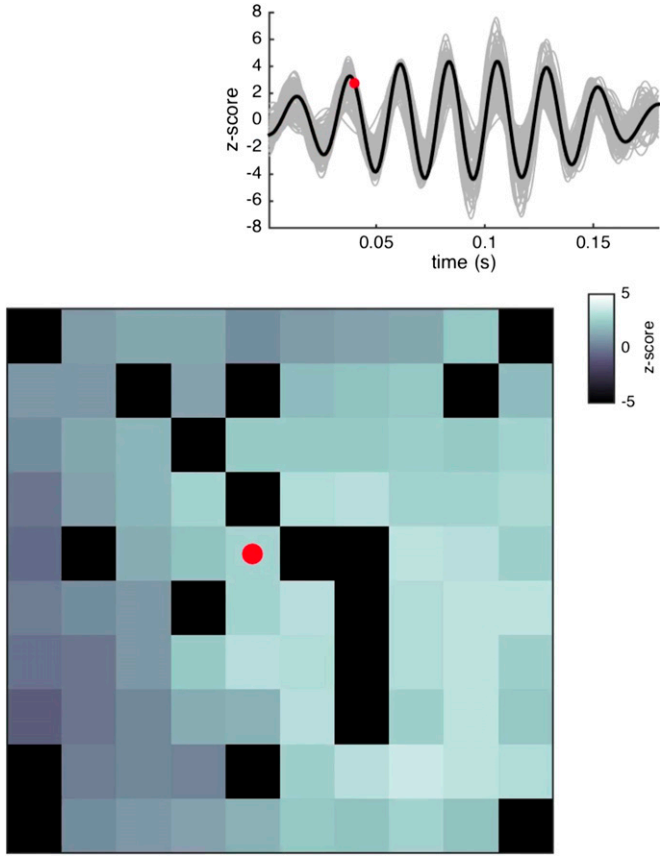

Movie S2. Example of a γ-frequency wave in human SWS. Data are plotted as in Movie S1.

Movie S2

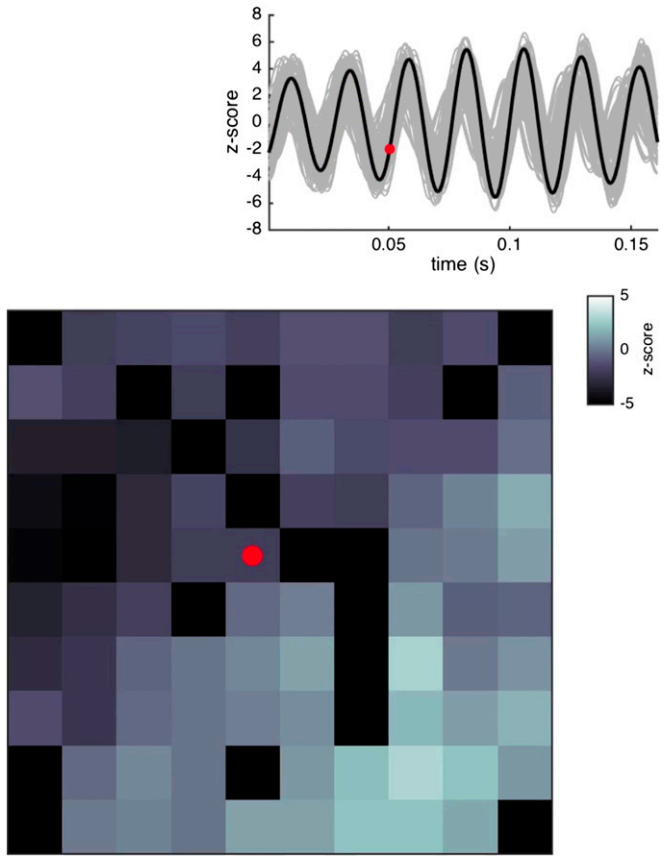

Movie S3. Additional example of γ-frequency wave in human SWS. Data are plotted as in Movie S1.

Movie S3